Journal of Bio- and Tribo-Corrosion (2024) 10:13
https://doi.org/10.1007/s40735-024-00818-4

New Insights on the Corrosion–Erosion Behavior of 904L Stainless Steel in Phosphoric Acid Containing Impurities

S. Aftimi[1] · Y. Kerroum[1] · A. Guenbour[1] · A. Bellaouchou[1] · H. Idrissi[2] · R. Boulif[3] · N. Semlal[3] · I. Warad[4] · A. Zarrouk[1]

Received: 9 July 2023 / Revised: 10 November 2023 / Accepted: 2 January 2024 / Published online: 27 January 2024

Abstract
This research aims to provide a new interpretation of the corrosion–erosion behavior of 904L stainless steel in a phosphoric acid environment, containing impurities promoting corrosion (4 wt% H_2SO_4, 0.42 wt% KCl) and solid particles favoring the mechanical effects. Electrochemical and spectroscopic analyzes were performed in this investigation. The results showed that solid particle concentrations affect the passivity of stainless steel, which turns it into a less stable layer, proving an increase in corrosion kinetics and passive current density. During this process, the passive film formed under these corrosion–erosion conditions presents a strong diffusion of metallic vacancies and the difficulty of self-healing of the passive film, the results of gravimetric measurements at 24 g/L of solid particles showed that this is due to the synergistic effect which has about 50%, and the mechanical effects have about 46%, of which the surface analysis proved that the surface became heterogeneous and rough.

Keywords 904L stainless steel · Corrosion–erosion · Phosphoric acid · EIS · XRD/UV–VIS–NIR/SEM/EDX

1 Introduction

The wet manufacture of phosphoric acid employs a large variety of materials that support the whole of the interaction conditions. And this medium contains various impurities, such as chloride, fluoride, sulfate and sulfide, as well as solid particles of suspended gypsum which produces a corrosion–erosion effect. For this, we chose SiC particles because they are chemically inert and have sufficiently sharp shapes to cause efficient and reproducible erosion in the laboratory like solid gypsum particles in real processes. Subsequently, the material in question should have good resistance in a way that reduces the global maintenance charges. Normally, phosphoric acid is produced by the attack of phosphoric rocks with sulfuric or chloride acid under specific thermal conditions [1]. For that, the austenitic stainless steel 904L is used as conception materials such as propeller-type agitators, centrifugal pumps, and filtration pans, due to their spontaneous aptitude to create a passive protective layer on their surface[1–3]. But the equipment operating under hydrodynamic conditions is subject to frequent phenomena such as corrosion and erosion [2, 4–11]. The complexity of corrosion–erosion phenomena is related to the variety of parameters [6, 13–21] that are linked to:

- Environment: pH, chemical composition, temperature, rheology of the corrosive solution…
- The abrading particles: shape, size, hardness, concentration …
- The material characteristic: chemical composition, roughness, surface morphology…
- Hydrodynamic conditions: angle of impact, flow rates, flow type …

The corrosion–erosion of stainless steel in phosphoric acid has been widely studied. A considerable amount of research was concentrated on the impact of erosion on material passivation. They suggest that the presence of erosion deteriorates the protection of stainless steel against corrosion and influences

✉ A. Zarrouk
azarrouk@gmail.com

[1] Laboratory of Materials, Nanotechnology and Environment, Faculty of Sciences, Mohammed V University in Rabat, Av. Ibn Battouta, P.O. Box. 1014, Agdal-Rabat, Morocco

[2] Univ Lyon, INSA Lyon, Université Claude Bernard Lyon 1, CNRS, MATEIS, UMR5510, 69621 Villeurbanne, France

[3] R&D Chimie-OCP, Casablanca, Morocco

[4] Department of Chemistry, AN-Najah National University, P.O. Box 7, Nablus, Palestine

the rate of passive film formation which leading its self-healing delicate [22–24]. Much research showed that the presence of chemical impurities and fluid particles may enhance the erosion impact by a synergistic effect[25, 26]. For that, many works suggest that material loss is due to the electrochemical mechanisms plus the mechanical impact of erosion and the synergistic effect of both phenomena [25, 27, 28]. Nevertheless, 904L stainless steel in a phosphoric acid environment, containing impurities that promote corrosion, is still yet to be studied to understand its behavior under corrosion–erosion conditions.

First, in this research document, the impact of the fluid particles concentration on the electrochemical parameters of 904L stainless steel is evaluated. Then a gravimetric study is carried out, to ensure that the synergistic effect of corrosion and erosion is approached, and finally, the characterization of the surface using different techniques is achieved with and without erosion.

2 Experimental Details and Methods

2.1 Material, Test Solution and APPARATUS

2.1.1 Material

Table 1 present the chemical composition of the stainless steel used in this study UNS08904 known as 904L also as UB6 cylindrically shaped with an area of 0.64 cm^2 exposed to the electrolyte. Before the tests, the specimen was ground with a series of SiC grit papers (180 up to 1500).

2.1.2 The environment

40 wt% H_3PO_4 solution polluted with 4 wt% H_2SO_4 and 0.42 wt% KCl(0.2 wt% Cl^-). The solid particles used are SiC hardness of 9.5 on the Mohs scale, sized of 210 µm with different concentrations of 6 g/L; 12 g/L; 24 g/L; and 30 g/L.

2.1.3 The apparatus

Figure 1 the experimental rig used in this study is composed of a:

- A Pyrex glass cell with two sides coaxial orifices: the first one allows a normal (90°) injection of the solution with and without solid particles. The second one is the recess of the working electrode to the cell.

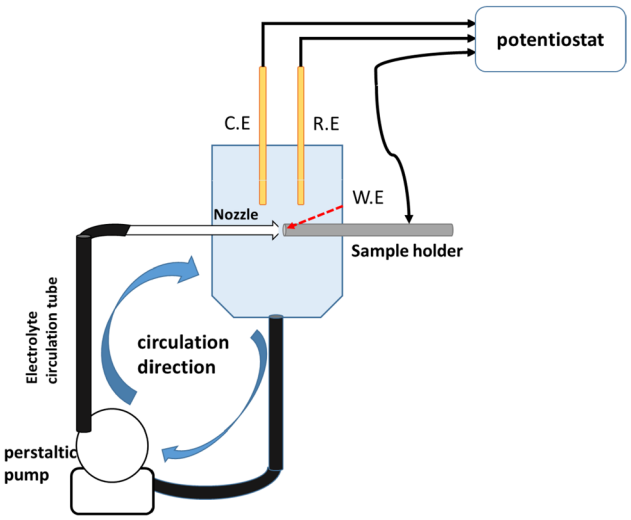

Fig. 1 Experimental rig for the corrosion- erosion tests (A.E: auxiliary electrode, R.E: reference electrode; W.E: Working electrode)

  - o The cover of the cell has recesses for the auxiliary electrode (Pt) and for the reference electrode (SCE), which are linked to the potentiostat/galvanostat (OrigaFlex—OGF01A), monitored with the Origamaster software.

- A peristaltic pump to ensure the circulation of the fluid and the velocity of the impinging jet is stated at the value of 2 m/s.
- The solid fraction of the slurry (state by mass) was quantified at 0.583%wt; 1.161%wt; 2.445%wt; and 3.009%wt.

2.2 Electrochemical Measurements and Characterization Techniques

The experimental study is divided into two parts. The first part, by using three electrodes, auxiliary electrode (platinum), reference electrode (saturated calomel electrode); Working electrode (W.E), the response of the stainless-steel sample to the impingement of the corrosive solution with different solid particle concentrations (6 g/L; 12 g/L; 24 g/L; and 30 g/L) was evaluated using the electrochemical techniques. The chrono-potentiometry was evaluated for 1800s, then the electrochemical impedance spectroscopy was performed at the corrosion potential that registered at the last time of chrono-potentiometry, with AC signals of amplitude 10 mV peak to peak, from 100 kHz to 100 mHz. The polarization curves were

Table 1 Chemical compositions of 904L stainless steel

Elements	Fe	Cr	Ni	Mo	Cu	Mn	C	Si	P	S	W
Wt%	Bal	20.77	25.09	4.37	1.50	1.84	0.01	0.15	0.03	0.01	0.13

plotted at the scan rate of 1 mV/s, and the chron-amperometry was applied at potential $E_p = +600$ mV/SCE.

Then in the second part, the gravimetric study under corrosion–erosion conditions was established at the free corrosion and cathodic potential application, aiming to evaluate the synergistic effect of corrosion and erosion phenomena. The effect of solid particles on the surface properties was revealed using characterization techniques after an immersion of 4 h in the hydrodynamics conditions: Scanning electron microscope and energy-dispersive spectroscopy analysis (SEM) JEOL JSM-IT 100 equipped with an EDX with an accelerating voltage of 20 kV that allows the observation of the morphology plus a quantitative analysis of the element on the alloy surface; the UV–visible spectroscopy (UV–VIS) deploying the (model Jasco V670) equipped with a 150 mm integrating sphere (model ILN-925)that allows the discrimination of the chemical elements on the surface; also the X-ray diffraction (XRD). Shimadzu 6100 diffractometer equipped with a copper anti-cathode (λCuKα = 1.541838 Å), a thin film attachment THA- 1101, and counter monochromator CM-4121. The samples were scanned at a speed of 2.0°/min between 20° and 110° (2θ) at a tube voltage of 40 kV and a current of 30 mA.

3 Results and Discussions

3.1 Chrono-Potentiometry

Figure 2 summarizes the results of the chrono-potentiometry that elucidate the variation of the corrosion potential as a function of time of stainless steel in 40 wt% phosphoric acid polluted by Cl^-, SO_4^{2-} ions in the presence of different concentrations of solid particles.

In the absence of solid particles, it can be seen that the potential enhances to a passive state throughout the first 400 s of immersion. Nevertheless, in presence of solid particles, with the concentration of 6 g/L, 12 g/L, 24 g/L, and 30 g/L we notice that corrosion potential increases throughout the first 60 s of immersion and it's declining down to constant values. Which can propose that the alloy forms a non-stable passive layer that is distracted in that aggressive conditions and the formation of another stable layer[29, 30]. Furthermore, the value of the corrosion potentials stabilizes shortly after the start of the test. And, the corrosion potential drop to less noble remains stable through time proposing that the aptitude to form a passive layer becomes more difficult.

Moreover, without solid particles, the corrosion potential becomes ennobled over time, confirming that the (904L) stainless steel spontaneously forms a passive layer on the surface, preventing the alloy from contacting the corrosive substances, due to the presence of an important percentage of chromium and nickel in the metal composition[31]. It can be concluded that, with the corrosion–erosion effect, the passivity of stainless-steel changes into a less stable layer and has a detrimental influence on the deterioration of the passivity in phosphoric medium.

3.2 Polarization Curves

Figure 3 illustrates the polarization curves of stainless steel in polluted 40% phosphoric acid in the presence of different concentrations of solid particles. The curves reveal that the alloy establishes a wide passivation range in both corrosion and corrosion–erosion. Furthermore, no activated peak was observed at all concentrations, this confirms that the alloy spontaneously forms the passive layer. The addition of solid particles dramatically changes the current density

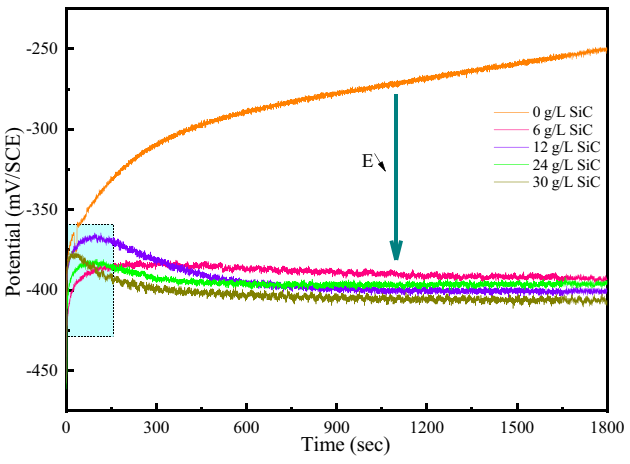

Fig. 2 Corrosion potential variation of 904L alloy in 40% phosphoric acid polluted with different percentages of solid particles

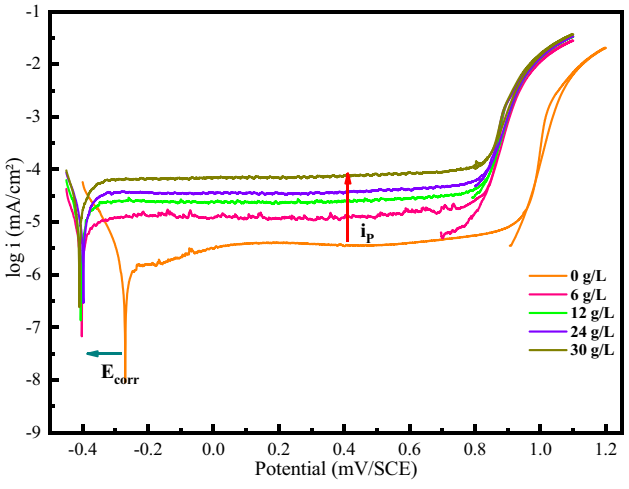

Fig. 3 Polarization curves of the alloy in polluted phosphoric acid in the presence of different percentages of solid particles

Table 2 Electrochemical parameters of the alloy in phosphoric acid polluted with Cl^- and SO_4^{2-} ions, in the presence of different percentages of the solid particles

Concentration (g/L)	i_{corr} (μA/cm^2)	E_{corr} (mV/SCE)	i_p (μA/cm^2)	E_{tr} (mV/SCE)
0	2.60	− 267	2.54	992.6
6	4.34	− 398	11.51	818.0
12	7.86	− 401	27.18	824.6
24	16.01	− 400	41.25	827.9
30	24.31	− 416	99.06	835.2

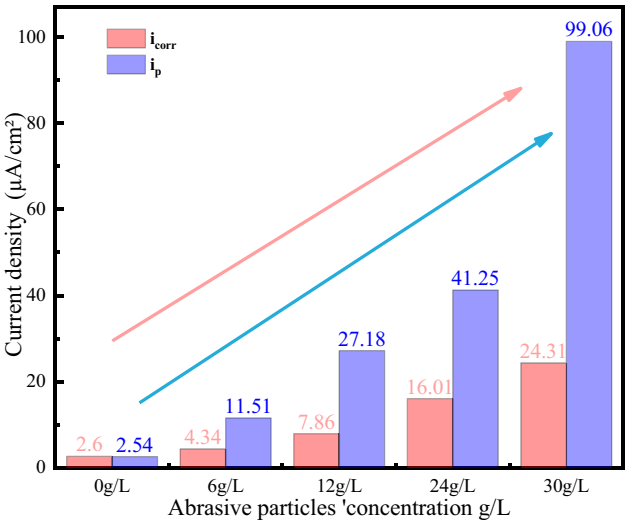

Fig. 4 Evolution of the corrosion and passivity current density of the alloy as a function of the concentration of solid particles in the 40% polluted H_3PO_4 solution

and corrosion potential of the alloy. Table 2 summarizes the electrochemical parameters of the polarization curves.

With the addition of solid particles, the corrosion potential changes to a less noble value from − 267 to − 419 mV/SCE, besides the transpassive potential reduces from 992.58 to 818 mV/SCE. Moreover, the addition of solid particles rises the current density to higher values, which multiplies the corrosion current density twice for the 6 g/L to twelve times for the 30 g/L (Fig. 4), proving that the kinetics of corrosion are elevated. Further, Fig. 4 points out that the current density of passivity is expanded five times for 6 g/L to 45 times for the 30 g/L. Many authors are interested in the way the passive film of stainless steel was established, the synergistic effect was verified between the alloying elements in particular Cr, Ni, Mo, and Mn which allows the stabilization of the passivation [31–38].

Generally, passivation is the formation of hydrate complexes of metals that react with water enabling the formation of hydroxide phase that deprotonate to form an insoluble oxide film on the surface [34], but the presence of solid particles may disturb this process, by cutting or plastic deformation of the surface, which may influence the depassivation kinetics to become greater than that of the passivation[5]. On the other hand, another suggestion can explain this, the roughness of the surface that will increase with the increase of solid particles in the liquid, according to a recent research published by Chen et al. [39], using the point defect model, the surface roughness can deteriorate the quality of the passive film by increasing the carrier density, thereby reducing the self-healing of the passive film.

3.3 Electrochemical Impedance Spectroscopy

To verify the proposition mentioned above, the electrochemical impedance of the alloy in the polluted 40% phosphoric acid in relation to the concentration of solid particles was carried out and presented with the Nyquist and Bode presentations in Figs. 5 & 6.

The Nyquist diagram shows capacitive behavior whose diameter depends on the concentration of solid particles. On the other hand, increasing the concentration of particles reduces the impedance of the material. This is in agreement with the reduction of the impedance modulus in the low-frequency range at the Bode presentation. Withal, the value of the phase angle is less than 90° which decreases depending on the concentration of solid particles. Besides, adding solid particles reduces the value of the phase angle, which means that the surface becomes rougher and more heterogeneous [40]. Therefore, the electrochemical impedance of the electrode/electrolyte interface is far from being an ideal capacitor, typical for solid-state electrodes. Consequently, the impedance spectra prove the response of a passive system by the non-perfect loops.

Generally, when stainless steel is in contact with an electrolyte, the passive layer developed on the surface is the origin of the material protection. Furthermore, to simulate the electrochemical behavior of the alloy in the polluted phosphoric acid without and with the presence of corrosion and erosion phenomena, the experimental results of the electrochemical impedance were analyzed in terms of the equivalent electrical circuit and is presented in Fig. 7.

The circuit represents the behavior of the surface in the absence and the presence of the solid particles (Fig. 7). With R_s is the resistance of the electrolyte; R_1 is the passive film resistance and CPE is the constant phase element related to the capacitance of the passive film. The use of a CPE is necessary to take into account the non-ideal behavior of capacitive elements [41]. The impedance of the constant phase element CPE is expressed by the relation:

$$Z_{CPE} = \frac{1}{Q(j\omega)^a} \quad (1)$$

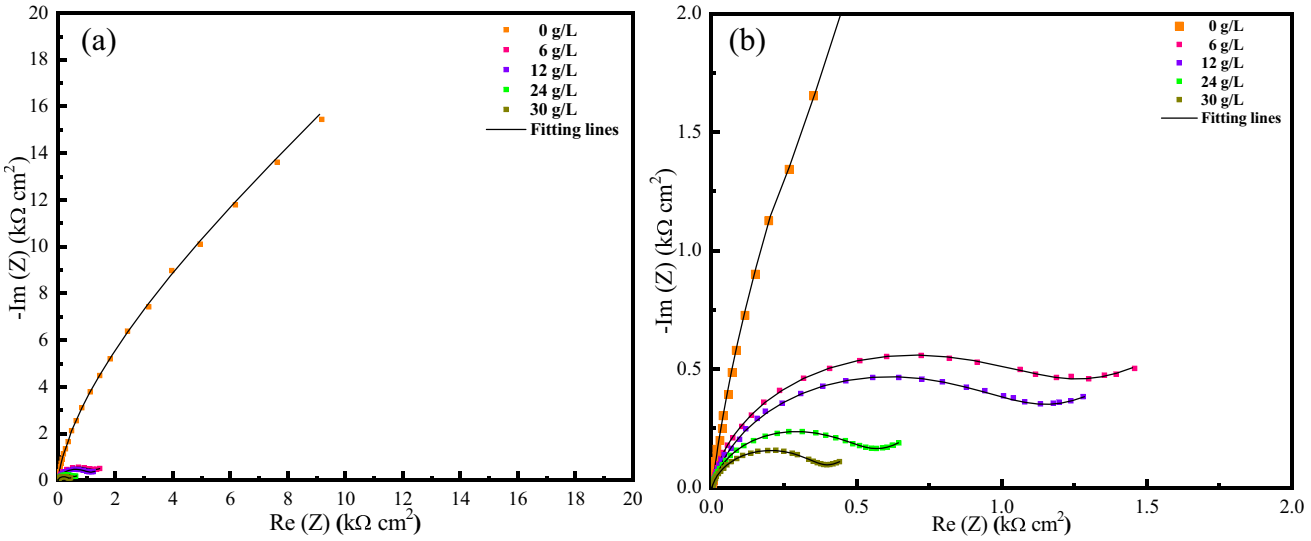

Fig. 5 Nyquist presentation of the electrochemical impedance spectroscopy of the alloy in the polluted 40% phosphoric acid (**a**) with and without solid particles, **b** the zoom of the Nyquist presentation in the presence of solid particles

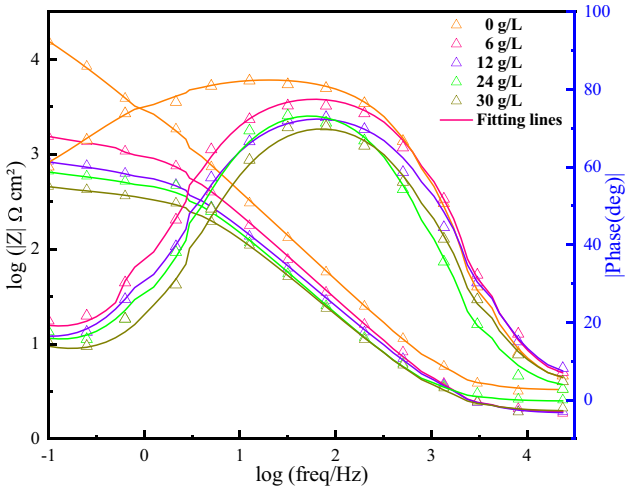

Fig. 6 Bode & phase presentation of the electrochemical impedance spectroscopy of the alloy in the polluted 40% phosphoric acid with and without solid particles

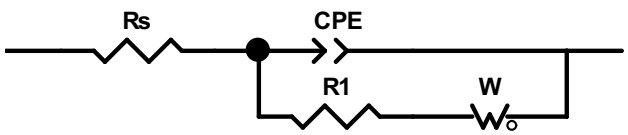

Fig. 7 Electrical circuit equivalent of the alloy surface in polluted phosphoric acid, with and without solid particles

Q is the CPE modulus when $\omega = 1$ rad/s, ω the radial frequency (rad/s), j the complex number: $j^2 = -1$ and 'a' is a characteristic parameter of the interface morphology, describing the non-homogeneity of the surface. The value of this positive exponent is less than 1. When $0.5 < a < 1$ implies that the use of the phase element constant is useful to simulate the non-ideal capacity [40]. Also, implies that the CPE describes a frequency dispersion of time constants due to local heterogeneity on the surface[42]. Besides, the Warburg impedance (Z_W) is a useful parameter in this circuit to explain the growth and damage of the passive layer that appears in the presence of the solid particles. In this investigation, this type of impedance represents the metal and the oxygen vacancies diffusion through the passive film [43]. Moreover, the transport of oxygen anion vacancies is negligible compared to the transport of metal cation vacancies in an aggressive environment[44], for that the Warburg impedance can be expressed as:

$$Z_W = \sigma_M \times \omega^{-1/2}(1 - j) \quad (2)$$

$\omega = 2\pi f$(rad s^{-1}), σ_M is the Warburg coefficient, which represents the diffusion resistance of metal cation vacancies through the passive layer.

Table 3 Parameters of the electrochemical impedance of the alloy in polluted phosphoric acid, with and without solid particles

Abrasive SiC(g/L)	R_s (Ω cm²)	Q (Ω^{-1} cm^{-2} s^a)	a	R_1 (Ω cm²)	σ_M (Ω $s^{1/2}$ cm^{-2})
0	3.26	50.86	0.937	11,520.00	14,437.00
6	1.89	94.59	0.911	1157.00	310.99
12	1.82	149.75	0.867	682.24	149.06
24	2.48	148.86	0.864	516.80	121.53
30	1.92	190.65	0.864	368.57	69.50

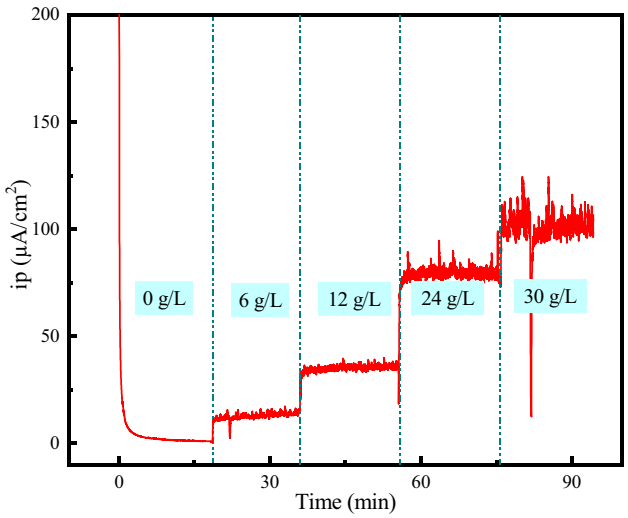

Fig. 8 Effect of the percentage of solid particles on the passive current density of the alloy in polluted phosphoric acid at E = 600 mV/SCE as a function of time

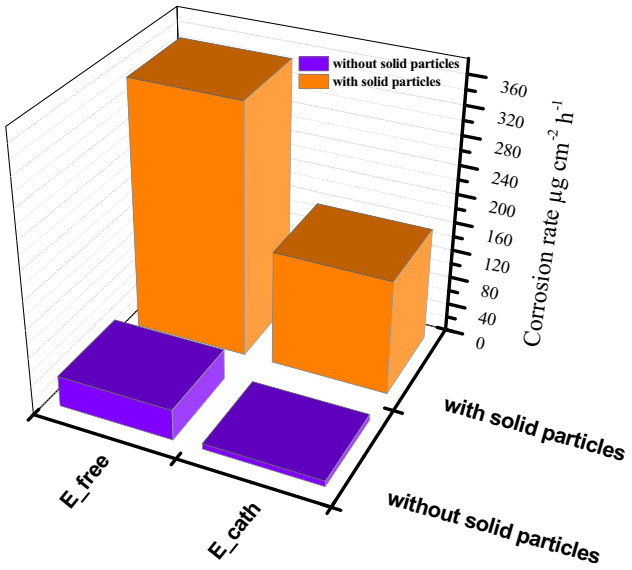

Fig. 10 The corrosion rate of alloy in 40% H_3PO_4 contaminated acid, with and without erosion (24 g/L)

Table 3 features the values of the different parameters of the equivalent circuit of the system under study. In absence of solid particles, the values extracted from the equivalent circuit presented in Fig. 7, show a high value of the Warburg coefficient and the resistance of the passive film indicating the presence of the compact and passive protective film. On the other hand, the addition of solid particles minimizes the value of the parameter 'a' meaning that the surface roughness is increased. And this leads to a significant decrease of R_1 from 11,520 Ω cm^2 to 368.57 Ω cm^2, which suggests that the passive film formed is more heterogeneous (less compact or destructed) [42, 44, 45]. Furthermore, according to the CPE values, the capacitance of the passive film will augment by about 4 times at 30 g/L. It is known that the CPE modulus is proportional to the permittivity and inversely proportional to the thickness of the passive film, the enhanced values could describe that the thickness of the passive layer is reduced [46] or have intense permittivity.

$$C = \frac{\varepsilon \varepsilon_0}{d} S \tag{3}$$

with: C = capacity; ε_0 = permittivity in vacuum; ε permittivity and d = film thickness.

Several authors [12, 21, 46–48] have studied the mechanisms of this damage, who have proposed that erosion can have at least three types of actions on the surface, ploughing and two types of cutting [10], including oxide film may be detached from the surface or subjected to the plastic deformation. Similar study was taken by Guenbour et al. [49], which explains the weakening of the passivation under the effect of erosion consists of an increase in mobile charge concentration and decrease of the thickness of the passive films.

Furthermore, this may also be due to the self-healing of the passive film has difficulty in erosion-corrosion conditions. The indicated proposition may be justified by, the value of the Warburg coefficient, the parameter decreases dramatically in the presence of the solid particles from 14,437 to 310.99 Ω s$^{1/2}$ cm^{-2} At 6% and to 69.50 Ω s$^{1/2}$ cm^{-2} at 30%, which implies that the diffusivity of metal cation vacancies in the passive layer is progressively increased. Depending on the point defect model [44], in corrosive medium, the high-cation vacancy diffusivity may cause the condensation of cation vacancies at the metal/film interface

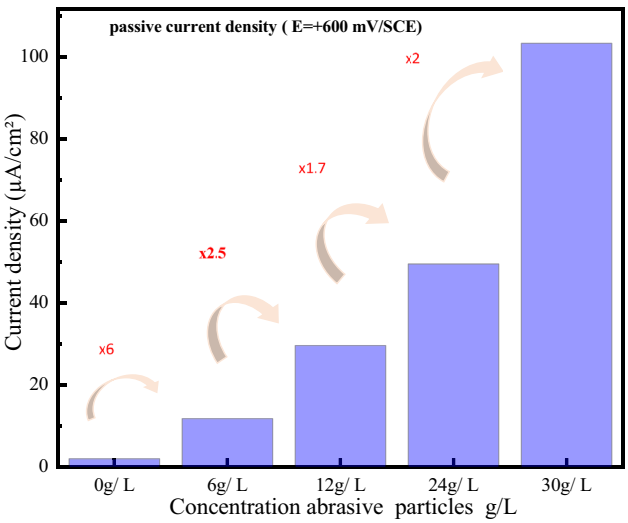

Fig. 9 Passive current density at the applied potential 60 mV/SCE as a function of the concentration of solid particles

Table 4 Corrosion rate and weight loss of the alloy during corrosion- erosion in 40% polluted phosphoric acid in presence of 24 g/L of solid particles

Alloy	EW	i_{corr} μA/cm^2	Δm_{elec} g m^{-2} j^{-1}	Δm_{mec} g m^{-2} j^{-1}	Δm_{tot} g m^{-2} j^{-1}	$\Delta m_{synergy}$ g m^{-2} j^{-1}
	23.95	16.01	3.43	38.44	84.38	42.51
Percentage			4.06%	45.56%	100%	50.38%

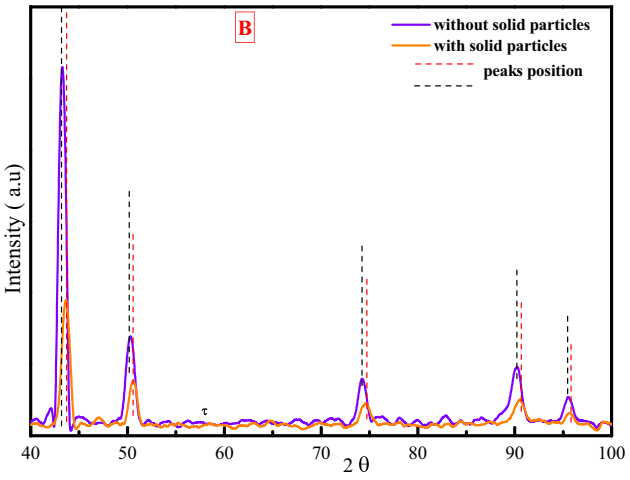

Fig. 11 X-ray diffractograms of the alloy (A) in the 40% polluted phosphor display with and without the presence of solid particles(24 g/L) and its zoom(B)

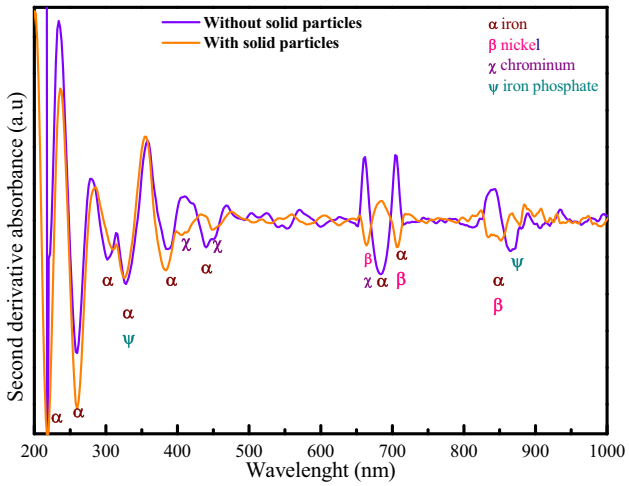

Fig. 12 The second derivative of the surface with and without erosion (24 g/L)

that inhibits the generation of oxygen vacancies, which reduce the film growth. However, under erosion-corrosion conditions, film thinning is mainly caused by the synergistic effect of two aspects, mechanical (hydrodynamics, contaminating particles) and electrochemical (corrosive medium) [50], and as this paragraph investigates the influence of the concentration of contaminant particles on the passive film, it can be considered that the film, for the most part, is eliminated mechanically. As a result, the surface roughness is increased, which may result in the formation of a passive film having a low resistance to diffusion of metal cation vacancies.

3.4 Chrono-amperometry

This mechanism of self-healing is studied at the applied potential $E_p = +600$ mV/SCE. Figure 8 illustrates the effect of the concentration of abrasive particles on the passive current density of the alloy in phosphoric acid polluted with Cl^- and SO_4^{2-} ions. We notice that in the absence of solid particles, the passive current density sharply drops and it attends the steady-state after few seconds which reflects the spontaneous passivity of alloy. It is also remarked that the passive current density rises after adding the solid particles (Fig. 9), notably, the fluctuations of the passive current density are enhanced with the concentrations of the particles, and it reaches the highest value at the concentration of 30 g/L. This provides information on that the self-healing mechanism of the passive film encounter difficulty when the concentration of solid particles is increased.

Generally, when stainless steel is exposed to solid particles, three processes contribute to this situation, the growth and the dissolution of the passive film and the mechanical damage [51]. Furthermore, the addition 6 g/L of abrasive particles enhances the passive current density values 6 times, then it is multiplied about 2 times after adding the other concentrations. This shows that the equilibrium of growth and dissolution of the passive film suffers from difficulties, especially as the current fluctuations are more pronounced at concentrations above 12 g/L, which explains that the concentration of 24 g/L is sufficient to study the impact of corrosion–erosion on the passive film.

Table 5 UV–VIS–NIR absorbance values of oxide compounds of the surface

Oxides	Degree of oxidation	Literature bands [nm]	Experimental wavelengths [nm]
Fe	II	825; 700 [54]; 820 [55]	708;
	III	373; 427 [54, 55] 250; 300 [56]	318; 425 259; 301
Cr_2O_3	III	460; 603 [57] 446; 548 [24] 410; 425 [56] 355; 570 [58] 200–700 [59]	683 440 and 470
Nickel	II	200–450; 410 [60]; 400 [61] 1400–900; 850–500; 550–370 [62] 844; 711; 492 [62] < 400	847
IRON PHOSPHATE		867 [63]; 225; 343; 365 [63] 230; 320 [64]	868; 340

3.5 Weight Loss Evaluation

The effect of 24 g/L solid particles on stainless steel in polluted 40%wt phosphoric acid was carried out at corrosion and cathodic potential. The total weight loss was measured before and after each test to calculate the corrosion rate. Using a Mettler Toledo balance (error = $\pm 1 \times 10^{-5}$ g) the weight loss was measured in the interest of calculating the corrosion rate from the relationship:

$$W\left(\mu g\, h^{-1}\, cm^{-2}\right) = \frac{\Delta m}{A \times t} \tag{4}$$

with Δm is the mass variation of samples after an immersion of the alloy in the dynamic conditions for a period (t) of 4 h; the contact surface A = 0.64 cm^2.

The corrosion rate is often expressed as a thickness lost versus unit time and can be calculated from corrosion current density or weight loss [22]. Figure 10 shows the corrosion rate of stainless steel in the presence and absence of 24 g/L solid particles at cathodic potential ($E_{\_cath}$), and corrosion potential (E_free). It is noted that in the presence of erosion, the corrosion rates are higher than those observed in the absence of erosion, in particular under the corrosion–erosion condition, which registers approximately 340 µg h^{-1} cm^{-2}.

Furthermore, to explain the rate of weight loss due to the synergistic effect during the corrosion- erosion conditions. Several authors have proposed that the total weight loss can be expressed as[9, 21, 22]:

$$\Delta m_{total} = \Delta m_{mechanical} + \Delta m_{electrochemical} + \Delta m_{synergetic} \tag{5}$$

With: Δm_{total} = The rate of total weight loss during immersion at corrosion potential; $\Delta m_{mechanical}$ = The rate of mechanical weight loss during the application of cathodic potential; $\Delta m_{electrochemical}$ = The rate of the weight loss due to electrochemical effect; $\Delta m_{synergetic}$ = The rate of weight loss due to the synergistic effect.

According to ASMT G102, the rate of the weight loss by electrochemical effect can be calculated by the Faraday equation:

$$\Delta m_{electrochemical} = MR\left(g\, m^{-2} j^{-1}\right) = K\, i_{corr} EW \tag{6}$$

With K is the conversion factor $8.954 \times 10^{-3} \left(\frac{g\, cm^2}{\mu A\, m^2\, j}\right)$, the corrosion current density is given by µA / cm^2, and EW is the equivalent mass of the unitless alloy[50].

Table 4 summarizes the corrosion rate and weight loss of the alloy during corrosion- erosion in 40% polluted phosphoric acid in presence of 24 g/L of solid particles. Generally, for stainless steels in polluted phosphoric acid, the rate of electrochemical corrosion is 3.56 g m^{-2} j^{-1} in order of 0.1 mm/year.

On the other hand, we observe from the gravimetric test results that the mechanical and the synergistic effects present 45.56% and 50.38%, respectively, and the electrochemical effect just represents 4.06% of the total weight loss of the alloy. So the fact that the total weight loss is governed by the synergistic effect, may be related to the mechanical effect that enhances the activation of electrochemical attack, especially in the presence of impurities such as chloride ions, this argument was found by Guenbour et al. [26] were suggested that the great significance

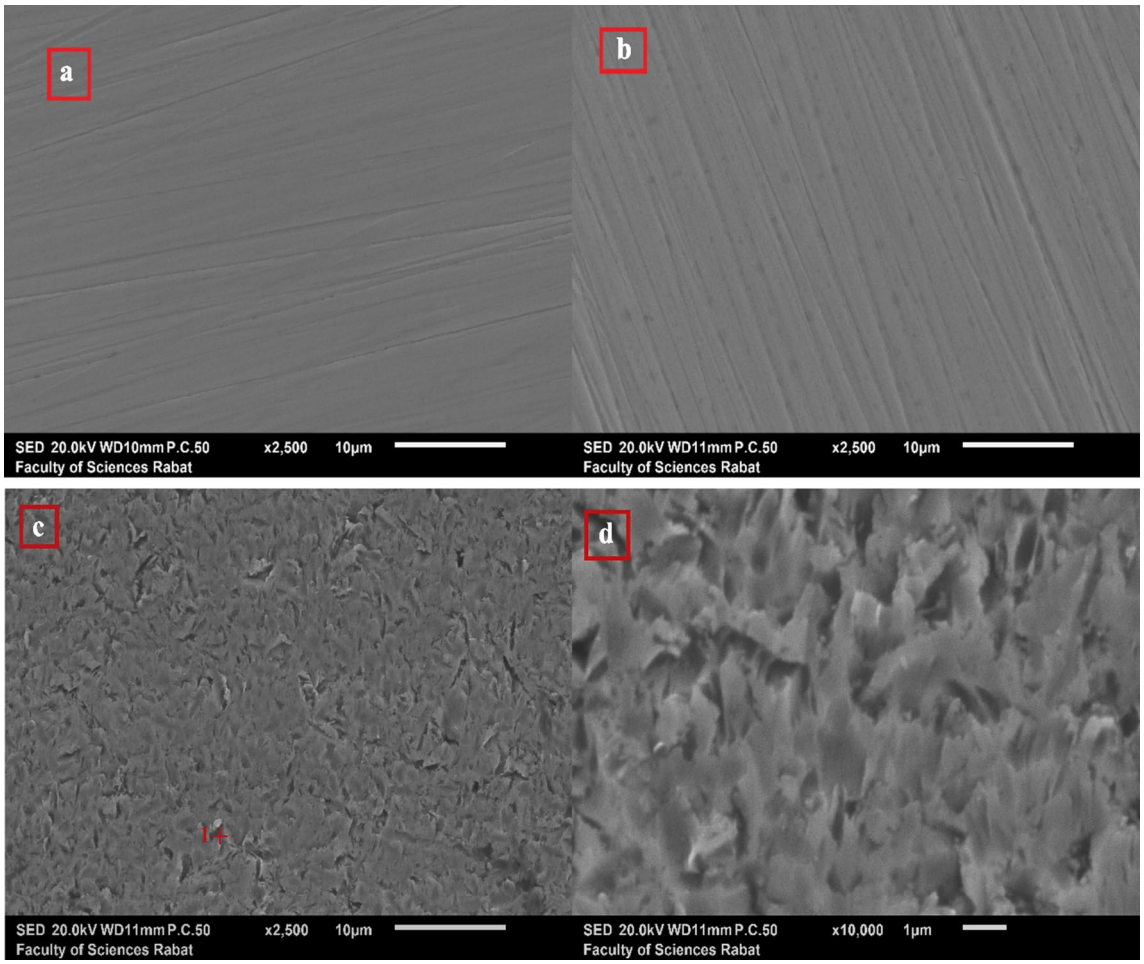

Fig. 13 SEM images of the surface of the alloy, **a** before test, **b** without erosion, **c** and **d** with erosion in polluted 40% phosphoric acid (24 g/L)

of the synergistic effect is mainly due to the combined activity of the solid particles and chloride ions.

3.6 Surface Characterization

3.6.1 XRD

XRD analysis can identify the atomic structure of crystals and surface compositions. The diffractogram of the alloy after immersion for 4 h in the presence and absence of solid particles.

(Fig. 11), showed that the five peaks γ (110), γ (200), γ (220), γ (311) and γ (400) related to the crystal structure of austenitic stainless steel[51–53], do not locate at the same angles of incidence.

Furthermore, it should be noted that the intensity of the XRD peaks of the alloy decreases after the addition of solid particles, which means that the roughness of the surface caused by the detached effect of the solid particles influences the surface properties.

3.6.2 UV–VIS–NIR

Figure 12 illustrates the results of the absorbance spectroscopy of the 904L stainless steel sample with and without the presence of solid particles; during this work we used the second derivative of the absorbance to demonstrate the chemical compositions of the surface.

The Fig. 12 indicates that the two surfaces have the same absorbance peaks, except for the amplitude, suggesting that the surface has almost the same chemical compositions. Table 5 resumes all the peaks related to the main elements and compounds that compose the surface, which is the iron with the second and third degree of oxidation on the wavelengths 708 nm and at 318, 425,259; 301 nm respectively. The nickel with a degree of oxidation number of + II, and the chromium (+ III) at the wavelengths 440,470 and 683 nm, also the iron phosphate at

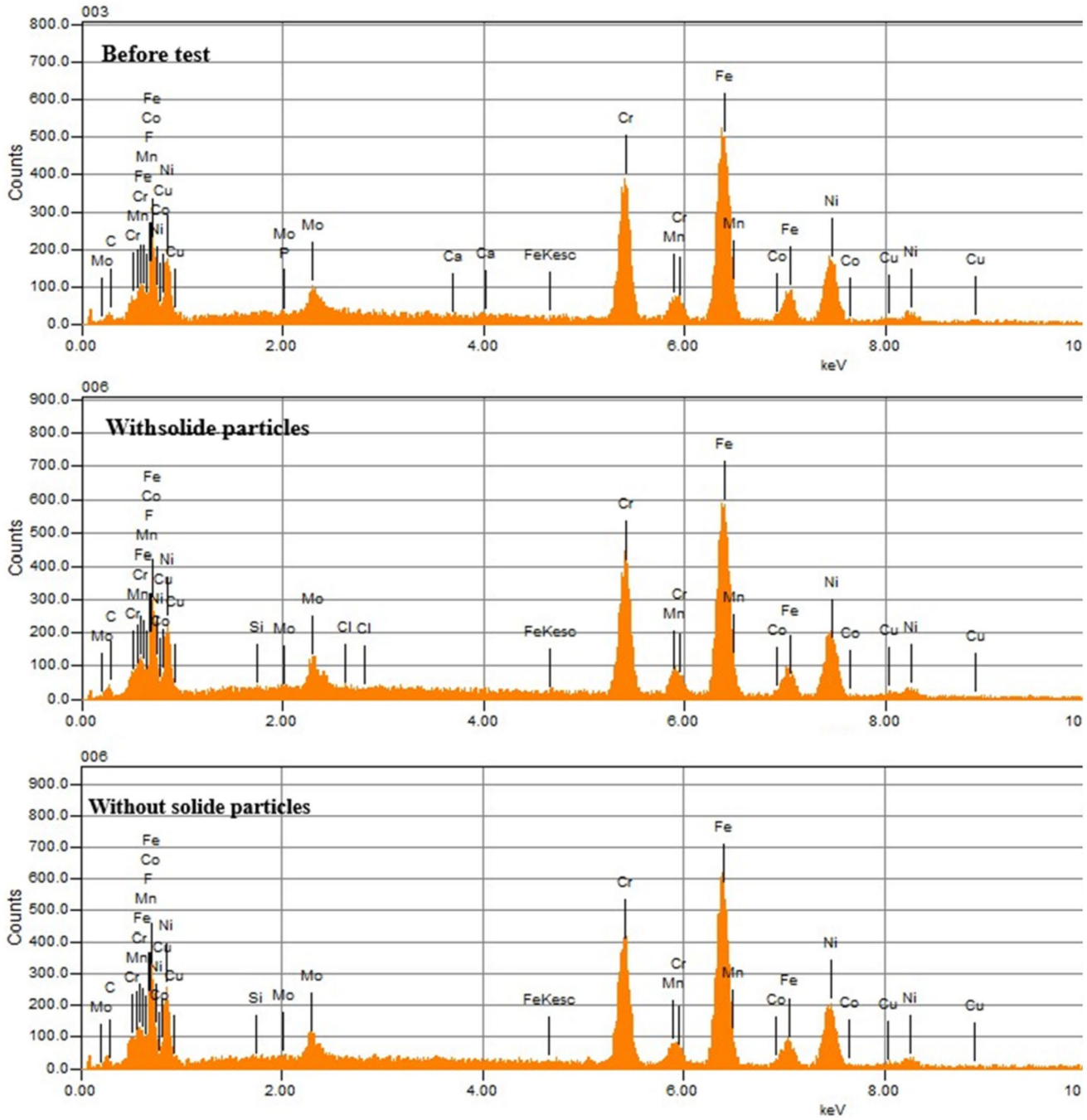

Fig. 14 EDX analyses of the alloy in 40% phosphoric acid polluted with and without solid particles

the wavelengths of 340 and 868 nm. From the graph, it is mainly observed that the amplitude of the iron and chromium peaks decreases in the presence of erosion, as a result, the continuous detached effect of solid particles decrease the amount of oxide on the surface. In addition, we mention here that surface roughness in erosion-corrosion conditions reduces the quality of the surface which can also affect the results of the absorbance spectroscopy.

3.6.3 MEB-EDX

The surface of the sample was observed before and after immersion in impure phosphoric acid with and without erosion (Fig. 13).

Figure 13a shows the alloy surface before the test, and Fig. 13b presents the surface of the material after immersion in the absence of solid particles, as observed, the material surface remains intact. Under corrosion–erosion conditions

(Fig. 13c, d), a random distribution of solid particle imprints was noticed on the surface, which means that the surface became heterogeneous and rough. Generally, the flow velocity brings kinetic energy to solid particles, which impose pressure on the surface, thus creating cavities, and creating a detached effect, this is clearly observed in Fig. 13d. Therefore, this may induce a decrease in the density of the oxides on the surface and difficulty of self-healing of the passive films as explained by EIS and chrono-amperometry analysis. Additionally, the continuous action of particles on the surface can cause fatigue or strains of the formed passive film and the base alloy.

The Figure above (Fig. 14) shows the EDX analyzes of the 904L alloy in polluted phosphoric acid and this under hydrodynamic conditions with and without solid particles. In general, there is no significant change in the chemical compositions of the surface of the alloy, but we note the appearance of chloride ions in results with solid particles, which suggests that ions of chloride are effectively adsorbed to the surface in corrosion–erosion conditions[50].

4 Conclusions

This research paper attempted to provide new information on the corrosion–erosion behavior of 904L (UB6) stainless steel, under hydrodynamic conditions of phosphoric acid contaminated with Cl^- and SO_4^{2-} ions, and with different concentrations of solid particles. The results proved that:

- The passivity of stainless-steel turns into a less stable layer with reduced corrosion potential.
- Corrosion current density and passive current density increase to higher values, indicating that the passive film has become less protective.
- The quality of the passive film deteriorates due to the low resistance to diffusion of metallic cation vacancies.
- The difficulty of passive film self-healing began to be more pronounced at concentrations of 24 g/L. whose mechanical and synergistic effects present 45.56% and 50.38%, respectively.
- SEM has proven that corrosion–erosion creates cavities and detachment effects which lead to the surface becoming heterogeneous and rough.

Acknowledgements The authors extend their appreciation to the OCP (Office Chérifien des Phosphates) foundation, to the Moroccan Ministry of Higher Education, Scientific Research and innovation (ENSSUP) and to the National Center for Scientific and Technical Research (CNRST) for funding and contribution to the realization of this work under the project APPHOS.

Author Contributions SA and YK: conceptualization; data curation; formal analysis; software; investigation; methodology; writing—original draft; writing—review & editing. AG, AB, HI, RB and NS: conceptualization; data curation; formal analysis; methodology; writing—original draft; writing—review & editing. IW and AZ: writing—original draft; writing—review & editing.

Funding There were no research Grants for this work from any funding agencies.

Data Availability All data generated or analyzed during this study are included in this published article.

Declarations

Competing interests The authors declare no competing interests.

Conflict of interest The authors declare there is no confict of interest regarding the publication of this article.

References

1. Schorr M, Valdez B (2016) The phosphoric acid industry: Equipment, materials, and corrosion. Corros Rev 34:85–102. https://doi.org/10.1515/corrrev-2015-0061
2. Boillot P, Peultier J (2014) Use of stainless steels in the industry: Recent and future developments. Procedia Eng 83:309–321. https://doi.org/10.1016/j.proeng.2014.09.015
3. BenSalah M, Sabot R, Triki E et al (2014) Passivity of Sanicro28 (UNS N-08028) stainless steel in polluted phosphoric acid at different temperatures studied by electrochemical impedance spectroscopy and Mott-Schottky analysis. Corros Sci 86:61–70. https://doi.org/10.1016/j.corsci.2014.04.056
4. Efremenko VG, Shimizu K, Noguchi T et al (2013) Impact-abrasive-corrosion wear of Fe-based alloys: Influence of microstructure and chemical composition upon wear resistance. Wear 305:155–165. https://doi.org/10.1016/j.wear.2013.06.006
5. Burstein GT, Sasaki K (2000) Effect of impact angle on the slurry erosion-corrosion of 304L stainless steel. Wear 240:80–94. https://doi.org/10.1016/S0043-1648(00)00344-6
6. Audouard J-P, Desestret A, Vallier G (1979) Comportement en corrosion-abrasion des aciers inoxydables spéciaux en milieux phosphoriques industriels. Matériaux Tech 67:439–450. https://doi.org/10.1051/mattech/197967120439
7. Guenbour A, Hajji M-A, Jallouli EM, Ben Bachir A (2006) Study of corrosion–erosion behaviour of stainless alloys in industrial phosphoric acid medium. Appl Surf Sci 253:2362–2366. https://doi.org/10.1016/j.apsusc.2006.05.005
8. Zeng L, Zhang GA, Guo XP (2014) Erosion-corrosion at different locations of X65 carbon steel elbow. Corros Sci 85:318–330. https://doi.org/10.1016/j.corsci.2014.04.045
9. Fan A, Long J, Tao Z (1996) An investigation of the corrosive wear of stainless steels in aqueous slurries. Wear 193:73–77. https://doi.org/10.1016/0043-1648(95)06684-5
10. Stack MM, Jana BD, Abdelrahman SM (2011) Models and mechanisms of erosion-corrosion in metals. Tribocorrosion Passiv Met Coat. https://doi.org/10.1016/B978-1-84569-966-6.50006-3
11. Rajahram SS, Harvey TJ, Wood RJK (2009) Evaluation of a semi-empirical model in predicting erosion-corrosion. Wear 267:1883–1893. https://doi.org/10.1016/j.wear.2009.03.002
12. Bitter JGA (1963) A study of erosion phenomena. Part II. Wear 6:169–190. https://doi.org/10.1016/0043-1648(63)90073-5
13. Maher M, Iraola-Arregui I, Ben Youcef H et al (2021) The synergistic effect of wear-corrosion in stainless steels: a review. Mater Today Proc. https://doi.org/10.1016/j.matpr.2021.05.010
14. Yi JZ, Hu HX, Wang ZB, Zheng YG (2019) On the critical flow velocity for erosion-corrosion in local eroded regions under

liquid-solid jet impingement. Wear. https://doi.org/10.1016/j.wear.2019.01.069
15. Xu X, van der Zwaag S, Xu W (2016) The scratch and abrasive wear behaviour of a tempered martensitic construction steel and its dual phase variants. Wear 358–359:80–88. https://doi.org/10.1016/j.wear.2016.04.005
16. Ojala N, Valtonen K, Heino V et al (2014) Effects of composition and microstructure on the abrasive wear performance of quenched wear resistant steels. Wear 317:225–232. https://doi.org/10.1016/j.wear.2014.06.003
17. Xu X, Xu W, Ederveen FH, van der Zwaag S (2013) Design of low hardness abrasion resistant steels. Wear 301:89–93. https://doi.org/10.1016/j.wear.2013.01.002
18. Ratia V, Miettunen I, Kuokkala VT (2013) Surface deformation of steels in impact-abrasion: The effect of sample angle and test duration. Wear 301:94–101. https://doi.org/10.1016/j.wear.2013.01.006
19. Neilson JH, Gilchrist A (1968) An experimental investigation into aspects of erosion in rocket motor tail nozzles. Wear 11:123–143. https://doi.org/10.1016/0043-1648(68)90592-9
20. Neilson JH, Gilchrist A (1968) Erosion by a stream of solid particles. Wear 11:111–122. https://doi.org/10.1016/0043-1648(68)90591-7
21. Bitter JGA (1963) A study of erosion phenomena: part I. Wear 6:5–21. https://doi.org/10.1016/0043-1648(63)90003-6
22. Watson SW, Friedersdorf FJ, Madsen BW, Cramer SD (1995) Methods of measuring wear-corrosion synergism. Wear 181–183:476–484. https://doi.org/10.1016/0043-1648(95)90161-2
23. Oltra R, Chapey B, Renaud L (1995) Abrasion-corrosion studies of passive stainless steels in acidic media: combination of acoustic emission and electrochemical techniques. Wear 186–187:533–541. https://doi.org/10.1016/0043-1648(95)07170-9
24. Skal S, Kerroum Y, Guenbour A et al (2019) Erosion-corrosion effect on the alloy 316L in polluted phosphoric acid. J Bio-Tribo-Corrosion 5:78. https://doi.org/10.1007/s40735-019-0270-4
25. Gou W, Zhang H, Li H et al (2018) Effects of silica sand on synergistic erosion caused by cavitation, abrasion, and corrosion. Wear 412–413:120–126. https://doi.org/10.1016/j.wear.2018.07.023
26. Guenbour A, Faucheu J, Ben Bachir A et al (1988) Electrochemical study of corrosion-abrasion of stainless steels in phosphoric acids. Corrosion 23:234–238. https://doi.org/10.5006/1.3583928
27. Pondicherry K, Fauconnier D, De Baets P (2020) Synergism in multi-asperity abrasion-corrosion of martensitic and dual phase steels in three aqueous electrolytes. Wear 452–453:203286. https://doi.org/10.1016/j.wear.2020.203286
28. Ferrer F, Idrissi H, Mazille H et al (2000) A study of abrasion—corrosion of AISI 304L austenitic stainless steel in sali PJne solution using acoustic emission technique. NDT E Int 33:363–371. https://doi.org/10.1016/S0963-8695(99)00061-4
29. Kerroum Y, Guenbour A, Bellaouchou A et al (2019) The corrosion of white cast iron in polluted phosphoric acid medium contains fluoride ions. Anal Bioanal Electrochem 11:497–509
30. Kim JJ, Young YM (2013) Study on the passive film of type 316 stainless steel. Int J Electrochem Sci 8:11847–11859. https://doi.org/10.1117/12.2084776
31. Sedriks AJ (1986) Effects of alloy composition and microstructure on the passivity of stainless steels. Corrosion 42:376–389. https://doi.org/10.5006/1.3584918
32. Guenbour A, Faucheu J, Ben Bachir A (1988) On the mechanism for improved passivation by addition of molybdenum to austenitic stainless steels in o-phosphoric acid. Corrosion 44:214–221. https://doi.org/10.5006/1.3583928
33. Maurice V, Peng H, Klein LH et al (2015) Effects of molybdenum on the composition and nanoscale morphology of passivated austenitic stainless steel surfaces. Faraday Discuss 180:151–170. https://doi.org/10.1039/c4fd00231h
34. Maurice V, Marcus P (2011) Adsorption layers and passive oxide films on metals. Tribocorrosion Passiv Met Coat. https://doi.org/10.1533/9780857093738.1.29
35. Sato N (1982) Anodic breakdown of passive films on metals. Electrochem Sci Technol 47:255–260. https://doi.org/10.3323/jcorr1991.47.78
36. Olefjord I, Brox B, Jelvestam U (1984) Surface composition of stainless steels during anodic dissolution and passivation studied by Esca. Proc Electrochem Soc 84–9:388–401. https://doi.org/10.1149/1.2113683
37. Olefjord I (1980) The passive state of stainless steels. Mater Sci Eng 42:161–171. https://doi.org/10.1016/0025-5416(80)90025-7
38. Rawers JC (2008) Alloying effects on the microstructure and phase stability of Fe–Cr–Mn steels. J Mater Sci 43:3618–3624
39. Chen J, Ma Y, Yin J et al (2021) Effect of surface roughness on the characteristics of passive film formed on 5083 Al alloy in pH 8.4 Borate Buffer Solution. Int J Electrochem Sci 16:1–10. https://doi.org/10.20964/2021.11.02
40. de Levie R (1989) On the impedance of electrodes with rough interfaces. Electroanal Chem 261:1–9. https://doi.org/10.1016/0022-0728(89)87121-9
41. Encinas-Sánchez V, de Miguel MT, Lasanta MI et al (2019) Electrochemical impedance spectroscopy (EIS): an efficient technique for monitoring corrosion processes in molten salt environments in CSP applications. Sol Energy Mater Sol Cells 191:157–163. https://doi.org/10.1016/j.solmat.2018.11.007
42. Escrivà-Cerdán C, Blasco-Tamarit E, García-García DM et al (2012) Effect of potential formation on the electrochemical behaviour of a highly alloyed austenitic stainless steel in contaminated phosphoric acid at different temperatures. Electrochim Acta 80:248–256. https://doi.org/10.1016/j.electacta.2012.07.012
43. Chao CY, Lin LF, Macdonald DD (1983) A point defect model for anodic passive films III. Impedance response. Electrochem Soc Electrochem Sci Technol 129:1874–1879. https://doi.org/10.1149/1.2124318
44. Macdonald DD (1992) The point defect model for the passive state. J Electrochem Soc 139:3434. https://doi.org/10.1149/1.2069096
45. Boudalia M, Guenbour A, Bellaouchou A et al (2013) Corrosion behaviour of a highly alloyed austenitic alloy UB6 in contaminated phosphoric acid. Int J Corros 2013:1–9. https://doi.org/10.1155/2013/363826
46. Bösing I, Bobrov I, Epp J et al (2020) Influence of systematically changed martensite content on the passive film properties of austenitic stainless steel in neutral electrolyte. Int J Electrochem Sci 15:319–333. https://doi.org/10.20964/2020.01.09
47. Tilly GP (1969) Erosion caused by airborne particles. Wear 14:63–79. https://doi.org/10.1016/0043-1648(69)90035-0
48. Finnie I (1960) Erosion of surfaces by solid particles. Wear 3:87–103. https://doi.org/10.1016/0043-1648(60)90055-7
49. Guenbour A, Bui N, Faucheu J et al (1990) The electrical properties of passive films formed on stainless steels in phosphoric acids. Corros Sci 30:189–199. https://doi.org/10.1016/0010-938X(90)90073-E
50. Du Y, Yang G, Chen S, Ren Y (2022) Research on the erosion-corrosion mechanism of 304 stainless steel pipeline of mine water in falling film flow. Corros Sci 206:110531
51. Barril S, Mischler S, Landolt D (2004) Influence of fretting regimes on the tribocorrosion behaviour of Ti6Al4V in 0.9 wt.% sodium chloride solution. Wear 256:963–972. https://doi.org/10.1016/j.wear.2003.11.003
52. Rajahram SS (2010) Erosion - corrosion mechanisms of stainless steel UNS S31603

53. ASTM G102-89 (1994) Standard Practice for Calculation of Information from Electrochemical Corrosion Rates and Related Measurements. In: Annual Book of ASTM standards, pp 416–422
54. Sanati A, Raeissi K, Edris H (2017) Investigation of the corrosion behavior of cathodic arc evaporated stainless steel coating in 3.5% NaCl. Prot Met Phys Chem Surf 53:902–909. https://doi.org/10.1134/S2070205117050197
55. Ziętala M, Durejko T, Polański M et al (2016) The microstructure, mechanical properties and corrosion resistance of 316 L stainless steel fabricated using laser engineered net shaping. Mater Sci Eng A 677:1–10. https://doi.org/10.1016/j.msea.2016.09.028
56. Kerroum Y, Guenbour A, Bellaouchou A et al (2019) chemical and physical effects of fluoride on the corrosion of austenitic stainless steel in polluted phosphoric acid. J Bio-Tribo-Corrosion 5:68. https://doi.org/10.1007/s40735-019-0261-5
57. Bunnag N, Kasri B, Setwong W, Sirisurawong E (2020) Study of Fe ions in aquamarine and the effect of dichroism as seen using UV – Vis , NIR and x-ray. 177. https://doi.org/10.1016/j.radphyschem.2020.109107
58. Chankhantha C, Kidkhunthod P (2016) Iron K-Edge Xanes Study of Heated Green Beryl from Madagascar Iron K -Edge Xanes Study of Heated Green Beryl from Madagascar. Walailak J Sci Technol 13:977–983
59. Kerroum Y, Skal S, Guenbour A et al (2018) Effect of fluoride on corrosion behavior of UNS N08904 stainless steel in polluted phosphoric acid. J Mol Liq. https://doi.org/10.1016/j.molliq.2018.06.008
60. Le Calvar M, Lenglet M (1989) UV-Vis-NIR and FTIR reflectance studies of the initial stage of oxidation of 80 Ni-20 Cr alloy. Stud Surf Sci Catal 48:575–580. https://doi.org/10.1016/S0167-2991(08)60718-1
61. Al-Buriahi MS, Alajerami YSM, Abouhaswa AS et al (2020) Effect of chromium oxide on the physical, optical, and radiation shielding properties of lead sodium borate glasses. J Non Cryst Solids 544:120171. https://doi.org/10.1016/j.jnoncrysol.2020.120171
62. Ali HE, Khairy Y, Algarni H et al (2019) The visible laser absorption property of chromium-doped polyvinyl alcohol films: synthesis, optical and dielectric properties. Opt Quantum Electron 51:1–12. https://doi.org/10.1007/s11082-019-1760-9
63. Annadurai K, Sudha V, Murugadoss G, Thangamuthu R (2021) Electrochemical sensor based on hydrothermally prepared nickel oxide for the determination of 4-acetaminophen in paracetamol tablets and human blood serum samples. J Alloys Compd 852:156911. https://doi.org/10.1016/j.jallcom.2020.156911
64. Hossain MI, Hasan AKM, Qarony W et al (2020) Electrical and optical properties of nickel-oxide films for efficient perovskite solar cells. Small Methods 4:1–10. https://doi.org/10.1002/smtd.202000454